Science of the Total Environment 735 (2020) 139559

Contents lists available at ScienceDirect

Science of the Total Environment

journal homepage: www.elsevier.com/locate/scitotenv

The impact of synoptic patterns on summertime ozone pollution in the North China Plain

Yueming Dong [a], Jing Li [a,*], Jianping Guo [b], Zhongjing Jiang [a], Yiqi Chu [c], Liang Chang [a], Yang Yang [d], Hong Liao [d]

[a] Department of Atmospheric and Oceanic Sciences, School of Physics, Peking University, Beijing 100871, China
[b] State Key Laboratory of Severe Weather, Chinese Academy of Meteorological Sciences, Beijing 100081, China
[c] Beijing Institute of Radio Measurement, Beijing 100871, China
[d] Jiangsu Key Laboratory of Atmospheric Environment Monitoring and Pollution Control, Jiangsu Collaborative Innovation Center of Atmospheric Environment and Equipment Technology, School of Environmental Science and Engineering, Nanjing University of Information Science and Technology, Nanjing 210044, China

HIGHLIGHTS

- Four synoptic patterns are identified via an objective classification method.
- The heaviest ozone pollution is related to an east high pressure center.
- A non-linear relationship between ozone and boundary layer height is noticed.
- Synoptic patterns are unlikely responsible for local increasing trend of ozone.

GRAPHICAL ABSTRACT

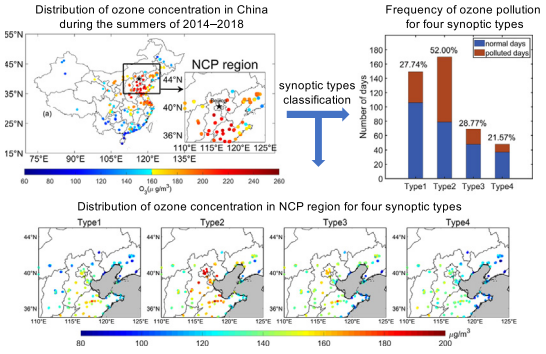

ARTICLE INFO

Article history:
Received 7 April 2020
Received in revised form 17 May 2020
Accepted 18 May 2020
Available online 19 May 2020

Editor: Jianmin Chen

Keywords:
Ozone pollution
Synoptic circulation
Effects of meteorological conditions
T-PCA classification method

ABSTRACT

Surface ozone pollution is a challenging environmental issue in most parts of China. In particular, the North China Plain (NCP) region suffers from the severest ozone pollution throughout the country. In addition to the emission of precursors, ozone concentration is closely related to meteorological conditions resulting from regional atmospheric circulation. In this study, we investigate the relationship between synoptic patterns and summertime ozone pollution in the NCP using the objective principal component analysis in T-mode (T-PCA) classification method. Four dominant synoptic patterns are identified during the summers of 2014–2018. The heaviest ozone pollution is found to be associated with a high pressure anomaly over the Northwest Pacific and a distinct low pressure center in Northeast China. The southwesterly wind surrounding the low pressure center brings dry, warm air from inland South China, resulting in a high temperature, low humidity environment in the NCP, which favors the chemical formation of surface ozone. Locally, this type is associated with a moderate planetary boundary layer height (PBLH) of ~860 m and a stronger warm anomaly within the boundary layer than the upper level. We also notice a non-linear relationship between surface ozone concentration and the PBLH, i.e., ozone concentration first increases with PBLH till ~0.9 km, and then remains stable. This initial increase may relate to enhanced mixing with upper levels where ozone concentration is typically higher than that near the surface. However, when PBLH further increases, this downward mixing effect is balanced with the stronger upward turbulent mixing so that surface ozone shows little change. The synoptic patterns identified here, however, is unlikely responsible for the observed increasing trend in ozone concentration over the NCP region. Our study sheds light on the meteorological contribution to surface ozone pollution in North China and provides a reference for the pollution control and prediction.

* Corresponding author.
E-mail address: jing-li@pku.edu.cn (J. Li).

https://doi.org/10.1016/j.scitotenv.2020.139559
0048-9697/

1. Introduction

The North China Plain (NCP) contains the biggest urban conglomerate in China and is one of the most densely populated regions in the world. With its rapid economic development, the NCP region also suffers from serious air pollution as a consequence of huge amounts of anthropogenic pollutant emissions, accumulation and regional transport (Chan and Yao, 2008; Ding et al., 2009; Gao et al., 2011; Zhang et al., 2012). In particular, surface ozone pollution has aggravated in NCP region in the past few decades and has exceeded $PM_{2.5}$ (particulate matter with aerodynamic diameter equaling to or <2.5μm) to become the primary pollutant in summer since 2014 (Wang et al., 2017, http: // www.cnemc.cn).

Ground-level ozone is an important trace gas that impairs air quality directly because its strong oxidizing property can cause serious damages to humans, animals and vegetation (Goodman et al., 2015; Mills et al., 2018). As the dominating element of photochemical smog, troposphere ozone is a kind of secondary pollutant formed through complex photochemical reactions of nitrogen oxides (NO_x) produced by fuel combustion, volatile organic compounds (VOCs) from both anthropogenic and biogenic sources, and other precursors (Zhang et al., 2014; Xue et al., 2014).

In addition to the amount of ozone precursors, the production of surface ozone critically depends on the meteorological conditions (Gao et al., 2005; Ding et al., 2008). A great deal of studies have demonstrated the importance of local meteorological variables on the concentration of surface ozone. For example, high temperatures can exacerbate photochemical smog mainly by accelerating the decomposition of peroxyacetylnitrate (PAN) and promoting biogenic emissions of isoprene (Jacob and Winner, 2009). A statistical analysis of 21 years of observations across the rural eastern U.S. indicates that the slope of ozone-temperature positively correlated relationship increases with increasing ozone precursor emissions (Bloomer et al., 2009). Wind direction is also an important factor which can lead to a high ozone concentration in downwind locations. Wang et al. (2001) found that weak westerly winds often result in ozone episodes in coastal Pearl River Delta cities like Hong Kong by transporting pollution from the inland cities. The change of local meteorological variables, on the other hand, is largely controlled by synoptic circulation patterns. Therefore, many previous studies focused on understanding the impact of these synoptic patterns on surface ozone pollution (e.g., Dayan and Levy, 2002; Hegarty et al., 2007; Demuzere et al., 2009; Liu et al., 2019a; Zhang et al., 2013). Shen et al. (2015) found that the ozone peaks in the Southeast United States can be explained by the variability of Bermuda High whereas the ozone peaks in the Northeast is related to the polar jet activity. Santurtún et al. (2015) demonstrated that ozone episodes in Spain often occur when the region is at the center of continental anticyclones which bring abundant solar radiation and light winds. In coastal regions, studies previously showed that subsidence airflow at the outskirts of low pressure systems like tropical cyclone usually leads to strong sunlight, high temperature and breeze that are conducive to ozone production and accumulation (Jiang et al., 2015). Similar studies have been conducted in other mid-latitude regions including the United Kingdom (Pope et al., 2016), central eastern China (Yang et al., 2014) and the Yangtze River Delta region in China (Ding et al., 2013; Camalier et al., 2007), highlighting the importance of investigating the relationship between ozone pollution and regional circulations.

Over the NCP region, there have also been increasing studies on the meteorological condition associated with surface ozone pollution. Lu et al. (2019a) used the GEOS-Chem model to show that ozone episodes in Beijing are typically associated with high temperature, which leads to intensive biogenic VOC emissions and efficient ozone production from both background and anthropogenic sources. Gong and Liao (2019) indicated that ozone pollution in the NCP is primarily caused by two processes: (1) positive net chemical production associated with high temperature and low relative humidity; (2) horizontal advection linked to anomalous southerlies and downward air flow from 500 hPa to the surface. On climate timescale, the Eurasian teleconnection pattern (EU), induced by the Arctic sea ice variability, may also impact on surface ozone in North China (Yin et al., 2019a; Yin et al., 2019b; Yin et al., 2020). Zhang et al. (2016) also found the intensity of summer monsoon could influence inter-annual and inter-decadal variations of surface ozone by controlling the formation of cyclone/anticyclone related weather patterns. These studies indicate that synoptic or circulation patterns play critical roles in the formation of severe ozone pollution episodes in North China. Nonetheless, these studies focused either on a particular case, or on large scale climate teleconnections or subjectively selected ozone pollution days. There is still lack of an objective assessment of dominant synoptic or local circulation patterns that are responsible for the heavy ozone pollution.

To identify the prevailing circulation types in long seasons, synoptic pattern classification techniques can be used as powerful and efficient dimension reduction tools. They have been widely applied in environmental and atmospheric studies concerning the weather conditions driven by daily synoptic circulation variability (Cheng et al., 2001; Comrie and Yarnal, 1992). Typical classification methods include correlation methods, cluster analysis (e.g., k-means), principal component analysis (PCA), nonlinear methods such as neural networks, and so on (Huth et al., 2008). Demuzere et al. (2009) used the Lamb–Jenkinson method to acquire an eastern-flow weather type linking with ozone pollution events in Netherlands. The empirical orthogonal function (EOF) approach is applied into several studies to demonstrate dominant patterns of ozone pollution, decomposing original meteorological variables (Shen et al., 2015; Yin et al., 2019a). The classification techniques have also been applied to study the circulation patterns associated with particulate matter pollution (Zhang et al., 2012; Chen and Wang, 2015; Miao et al., 2017; He et al., 2018; Liu et al., 2019b). By examining the changes of meteorological variables under the circulation pattern with high PM concentrations, insights into the formation mechanism of heavy pollution conditions were gained. Inspired by these previous works, here we investigate the impacts of regional synoptic forcing on summertime ozone pollution in the NCP region through an objective circulation classification approach combined with a statistical distinguishability test. The meteorological conditions under different circulation patterns will be further analyzed to examine the relationship between ozone pollution and major meteorological variables, including temperature, relative humidity, wind direction and speed, total cloud cover, solar radiation, precipitation and planetary boundary layer height (PBLH). The paper proceeds in four sections, which aims at finding the dominant synoptic patterns and related meteorological conditions that lead to high ozone concentration. To be specific, Section 2 introduces the data and methodology used. In Section 3, the results of synoptic patterns and the associated meteorological anomalies are analyzed, and their relationships with ozone pollution are discussed. Section 4 presents a discussion of our results in the context of recent works and the increasing ozone trend. Finally, Section 5 concludes our main findings.

2. Data and methodology

2.1. Surface ozone observation

Continuous and systematic ozone observations in China became available since the establishment of the nationwide ozone monitoring network in 2013 (Wang et al., 2017). In our study, the maximum daily 8-h average (MDA8) ozone concentration is calculated using the hourly ground-level ozone concentration observations collected from 218 stations in the NCP region during the summers from 2014 to 2018 (data released by the China National Environmental Monitoring Centre and is made available at http://beijingair.sinaapp.com/). Regional ozone pollution in the NCP is defined when the averaged MDA8 ozone concentration of 218 stations is above 160$\mu g/m^3$, according to the Technical

Regulation on Ambient Air Quality Index of China published by the Ministry of Environmental Protection of China in 2012.

2.2. ECMWF reanalysis dataset

To identify the dominant synoptic patterns, we use mean sea level pressure (SLP) data from the European Centre for Medium-Range Weather Forecasts (ECMWF) ERA5 hourly reanalysis dataset (Copernicus Climate Change Service (C3S), 2017). The ERA5 reanalysis data is available each hour with a horizontal resolution of 0.25° × 0.25°. In this study, 00 UTC (08:00 Beijing Time, BJT) data was chosen to analyze the daily circulation patterns, because at this time the routine radiosonde data is assimilated to make the reanalysis data more accurate (Li et al., 2017). In addition, meteorological variables at 14:00 BJT when ozone concentration usually peaks are used, including temperature at 2 m (T2m), relative humidity (RH) at 950 hPa, wind fields at 950 hPa, total cloud cover (TCC), downward ultraviolet (UV) radiation at the surface and total precipitation.

2.3. Synoptic pattern classification

There are three major groups of classification approaches: subjective, hybrid and objective (Huth et al., 2008). Here we adopt the objective method where numerical procedures define the types and assign cases, because this method is superior in dealing with large volumes of data and less dependent on previous experiences. We use the recommended objective method by Huth et al. (2008), namely the obliquely rotated principal component analysis in the T-mode (T-PCA) approach, which has the advantage of being able to reproduce predefined types, being less dependent on pre-set parameters, and generating stable performance both temporally and spatially (Richman, 1981; Huth et al., 2008). The method organizes the data matrix into grid points in rows and time series in columns. Then the typical weather patterns can be found with the eigenvectors calculated by singular value decomposition. In this study, the cost733class software package (http://cost733.met.no) is applied to implement the T-PCA classification (Philipp et al., 2010), which has been widely used in previous studies (e.g., Zhang et al., 2012; Miao et al., 2017).

Here the T-PCA is applied to the SLP field covering 35–45°N, 110–125°E. A larger domain (15–60°N, 90–160°E) is further analyzed to better observe the background large scale circulation.

The keypoint of T-PCA is the determination of the optimal number of patterns. For this purpose, we consider a field of significance approach based on the "false discovery rate" (FDR, Benjamini and Hochberg, 1995; Wilks, 2006; Johnson, 2012). Compared to other conventional field significance tests, this approach has been found to have better test power, much higher computation efficiency, and robust results without having to assume that the variables are independent (Wilks, 2006). The FDR refers to the expected fraction of local null hypotheses rejections which are actually incorrect. Here our local hypothesis is whether the SLP anomalies at each grid point in pattern i are significantly different from those in pattern j. If at least a p value of one local test meets the specified FDR criterion (here we set q=0.05), the patterns produced by T-PCA are statistically distinguishable at the level q. If no test satisfies the criterion, the T-PCA results are not statistically indistinguishable. The detailed steps are provided below.

First, for each pair of T-PCA pattern i (j) with n_i (n_j) members, the p value at each grid point (latitude λ and longitude θ) is calculated corresponding to the Student's t distribution:

$$t(\lambda,\theta)=\frac{\overline{SLP}_i(\lambda,\theta)-\overline{SLP}_j(\lambda,\theta)}{S(\lambda,\theta)\sqrt{\frac{1}{n_i}+\frac{1}{n_j}}} \quad (1)$$

where $S(\lambda,\theta)$ can be derived as:

$$S(\lambda,\theta)=\sqrt{\frac{(n_i-1)S_i(\lambda,\theta)^2+(n_j-1)S_j(\lambda,\theta)^2}{n_i+n_j-2}} \quad (2)$$

In the equations, the variable $\overline{SLP}_i$ ($\overline{SLP}_j$) indicates the composite SLP for T-PCA pattern i (j), and S_i (S_j) is the standard deviation of all SLP anomalies within pattern i (j).

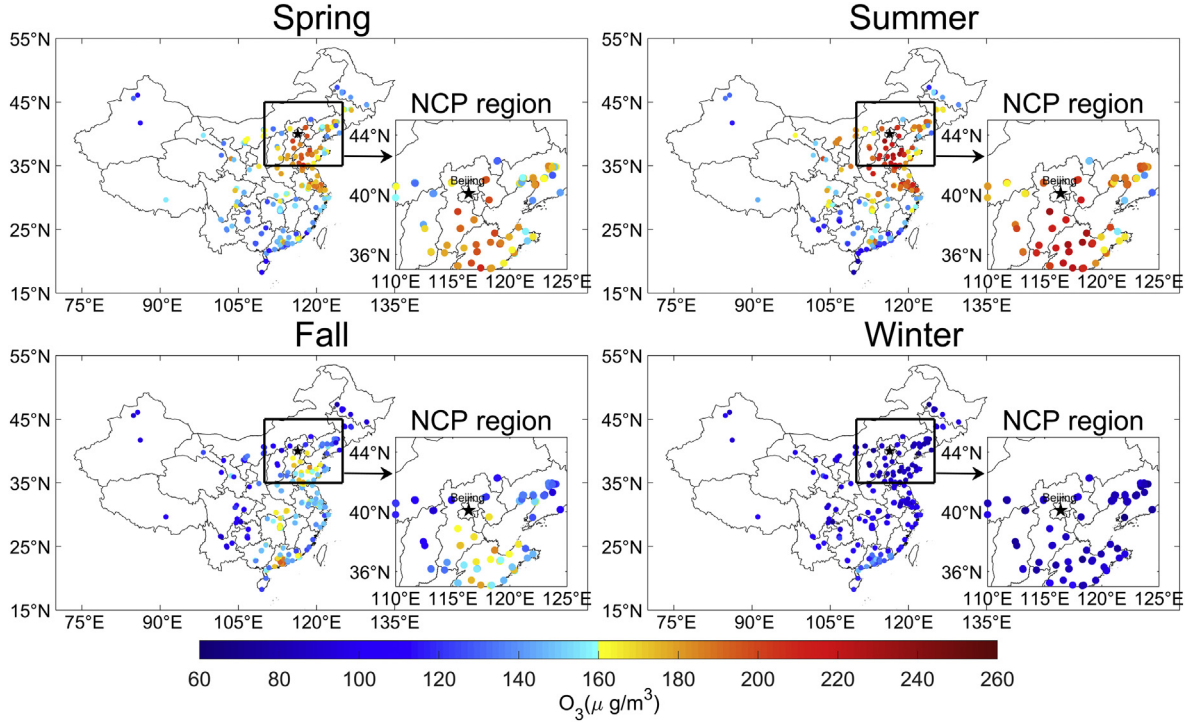

Fig. 1. Multi-year averaged seasonal 90th percentile values of the maximum daily 8-h average (MDA8) ozone concentration in China from 2014 to 2018.

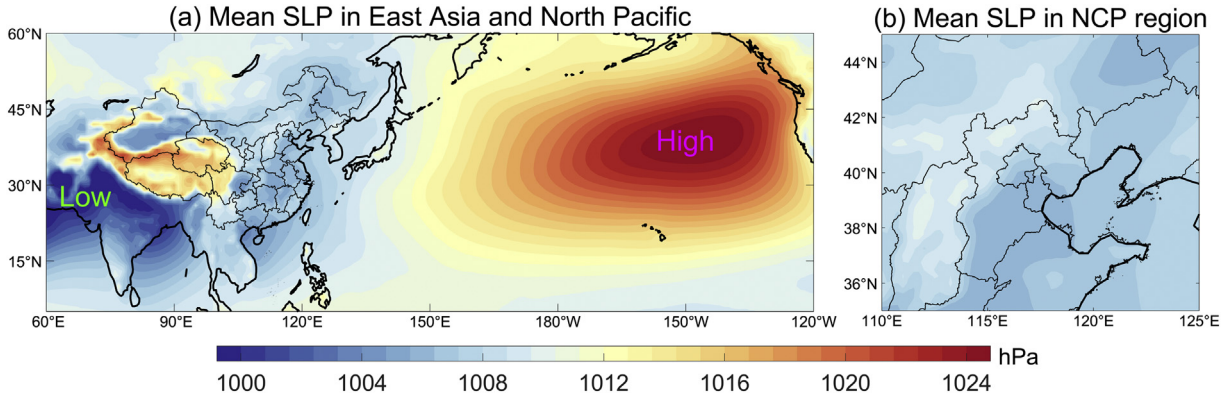

Fig. 2. a) Mean sea level pressure (SLP) over East Asia and North Pacific in summer during 2014 to 2018, with marked centers of low and high pressure systems; b) Mean summertime SLP in the NCP region from 2014 to 2018.

Then we obtain a distribution of M local p values (M represents the number of total grid points) for each pair of pattern i (j) via the calculation above, which will be evaluated by FDR tests to determine the critical p value controlling the FDR at the level $q = 0.05$. All p values are ranked in ascending order and p_m represents the mth smallest of the M local p values. The critical p value can be calculated as.

$$p_{FDR} = \max_{m=1,\ldots,M}\left[p_m : p_m \le q\left(\frac{m}{M}\right)\right] \tag{3}$$

If no local p values are smaller than or equal to p_{FDR}, the null hypotheses are true, which means the patterns are statistically indistinguishable. On the contrary, if any local test meets the criterion, the patterns are significantly distinguishable at the 5% level.

To determine the optimal number of patterns, we perform FDR tests for each choice of number K which increases from 2 to 10. For K T-PCA patterns, all $\frac{K(K-1)}{2}$ possible pairs of patterns are evaluated with FDR tests and the number of indistinguishable pairs will be counted. The optimal number of patterns is the maximum number of patterns without any statistically indistinguishable pair of patterns.

2.4. Radiosondes and PBLH calculation

We use the radiosonde data at the Beijing weather station (Station Number: 54511, 39.80°N, 116.47°E) provided by the China Meteorological Administration (CMA) to calculate PBLH. The L-band sounding system in the station provides fine resolution profiles of temperature, pressure, relative humidity, wind direction and speed twice a day routinely all the year, at 00:00 (08:00 BJT) and 12:00 UTC (20:00 BJT). During the summer monsoon season, an additional sounding 06:00 UTC (14:00 BJT) is launched daily (Guo et al., 2016). We thus use the soundings at 14:00 BJT to investigate the afternoon structure of PBL when it is close to be fully developed.

The bulk Richardson number (Ri) method (Vogelezang and Holtslag, 1996), as one of the most accurate techniques for PBLH estimation, is applied to estimate the PBLH in Beijing from sounding data. This method is suitable for both stable and convective boundary layers (Seidel et al., 2012). The Ri is defined as the dimensionless ratio of turbulence induced by buoyant suppression to that related to mechanical shear, expressed as follows:

$$Ri(z) = \frac{\left(\frac{g}{\theta_{vs}}\right)(\theta_{vz}-\theta_{vs})(z-z_s)}{(u_z-u_s)^2+(v_z-v_s)^2+(bu_*^2)} \tag{4}$$

where z is the height above the ground, subscript s denotes the surface, g is the acceleration of gravity, θ_v is the virtual potential temperature, u and v are the components of the horizontal winds, b is a constant (~100), and u_* is the surface friction velocity. We ignore u_* here because the magnitude of surface frictional effect is much smaller than that of the bulk wind shear term in the dominator (Vogelezang and Holtslag, 1996). Previous theoretical and laboratory studies show that the laminar flow becomes unstable turbulence as Ri becomes smaller than the critical value. Thus, the PBLH can be calculated as the lowest height (z) at which the interpolated Ri crosses the crital value (set to be 0.25, as suggested by Guo et al., 2016).

2.5. Backtrajectory calculation

We also compare the air mass transport features under different weather patterns by examining backward trajectories arriving at Beijing (39.80°N, 116.47°E) at 10 m above ground for a 48-h duration. The back trajectories are calculated by the Hybrid Single-Particle Lagrangian Integrated Trajectory model (HYSPLIT) developed by the National Oceanic and Atmospheric Administration (NOAA) Air Resources Laboratory (ARL) (https://ready.arl.noaa.gov/HYSPLIT.php, Draxler and Hess, 1998), which has been widely used in previous studies to stimulate atmospheric transport (e.g., Davis et al., 2010; Hegarty et al., 2009; Stein et al., 2015; Zhu et al., 2019).

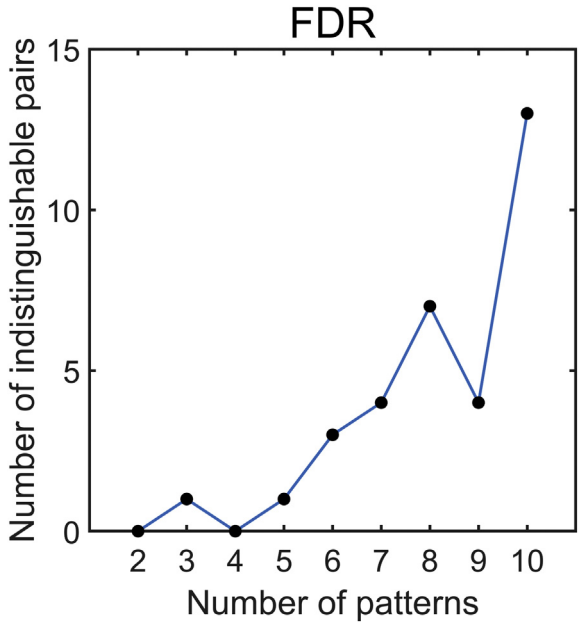

Fig. 3. The number of statistically indistinguishable T-PCA pattern pairs at the 5% significance level as a function of the number of T-PCA patterns.

3. Results

3.1. Seasonal variability of surface ozone pollution in the NCP area

Before analyzing the synoptic patterns, we first briefly overview the seasonal and spatial variability of ozone pollution in China. Fig. 1 depicts the multi-year averaged 90th percentile of seasonal MDA8 ozone in China during the period of 2014–2018. The warm colors (yellow to red) describes ozone pollution events with 90th percentile of MDA8 values exceeding 160$\mu g/m^3$. Ozone pollution in China exhibits substantial spatial and temporal variations. The highest surface ozone concentration is found in the NCP region (marked by black box), and the summertime (June, July and August) pollution is the worst among all seasons.

The seasonal variability mainly follows the change of solar radiation, i.e., increased UV radiation in the summer enhances ozone production. Other factors, such as the seasonality of clouds and precipitation (Ding, 1992; Chen et al., 2019), also play roles and explain the relatively lower MDA8 values for July and August, owing to the significant resultant reduction of insolation reaching at the land surface in the presence of clouds. Considering this seasonality of ozone pollution, next we focus on analyzing the circulation patterns during the summer months from June to August.

3.2. Synoptic pattern classification

The NCP is located in the East Asian Monsoon domain. In summer, the weather patterns are under the control of West Pacific Subtropical High (WPSH) pressure system (Wang et al., 2006; Zhao and Wang, 2017), adjusted by local topography related to sea-land and mountain-plain distribution. The mean circulation pattern over East Asia and North Pacific (from 5°N to 60°N and from 60°E to 120°W) in Fig. 2 shows the low pressure system (India Depression) prevails in East Asia continent, whereas the east to the NCP over the oceans is dominated by the WPSH.

To determine the optimal number of patterns, we perform the T-PCA classification on the SLP field with different number of clusters, and examine their FDR test results, as described in Section 2.3 (Fig. 3). It is seen that there is no indistinguishable pair of patterns for four clusters. But when the number increases, indistinguishable pairs will always be detected. We thus consider that four is the optimal number of clusters for our study.

Fig. 4 shows the SLP patterns as well as their anomalies for the four clusters identified by the T-PCA. The numbers on the top right corner indicate their frequencies of occurrence. The anomaly patterns are shown in two domains, i.e., the NCP region ranging from 35°N to 45°N and from 110°E to125°E, and a larger domain from 15°N to 60°N and from 90°E to

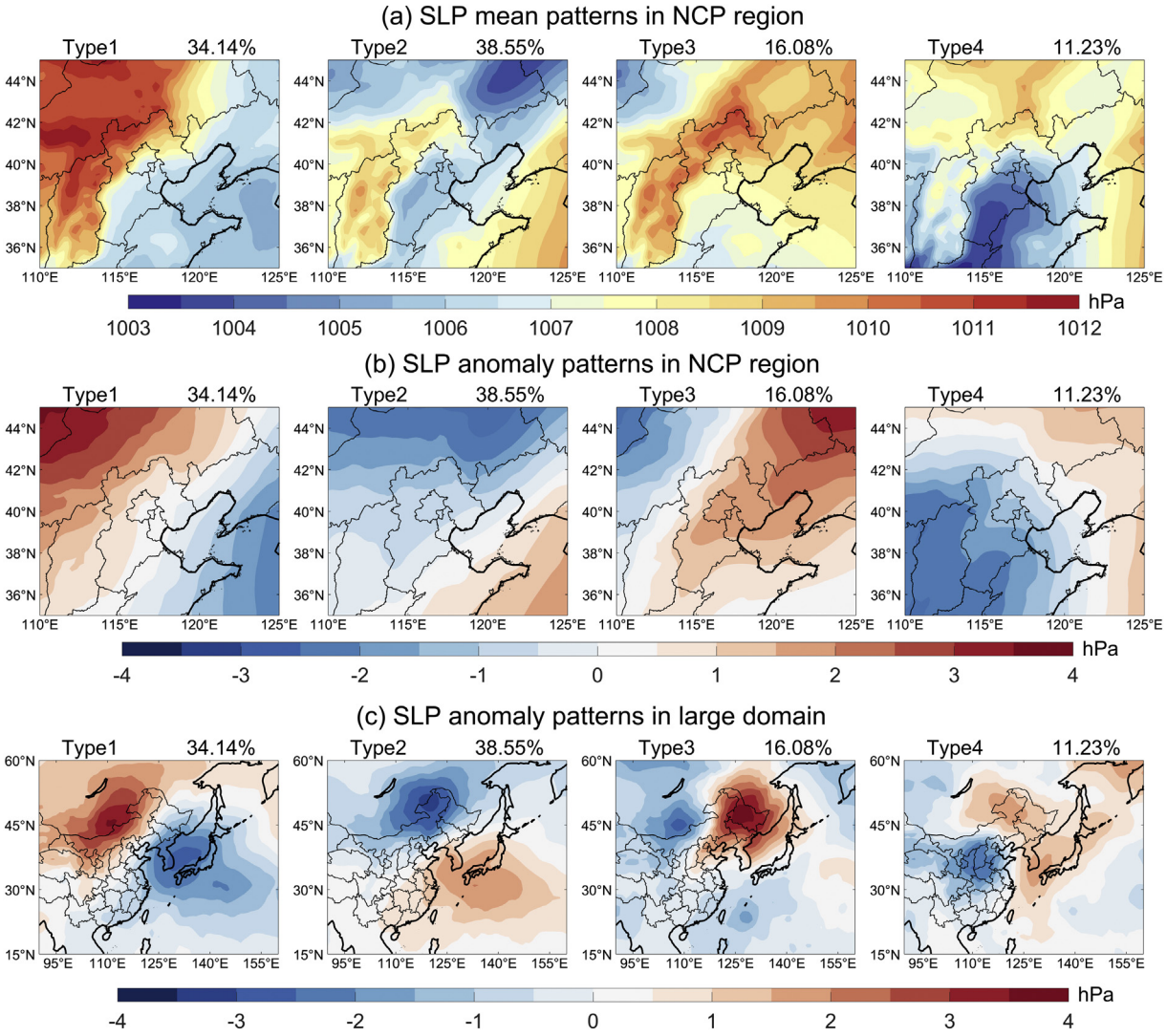

Fig. 4. a) Four composite sea level pressure (SLP) patterns for each circulation type in the NCP region in summer for 2014–2018; b) Anomaly patterns for each circulation type; c) Anomaly patterns in the large domain. The number at the upper right corner of each panel indicates the frequency of occurrence of each type.

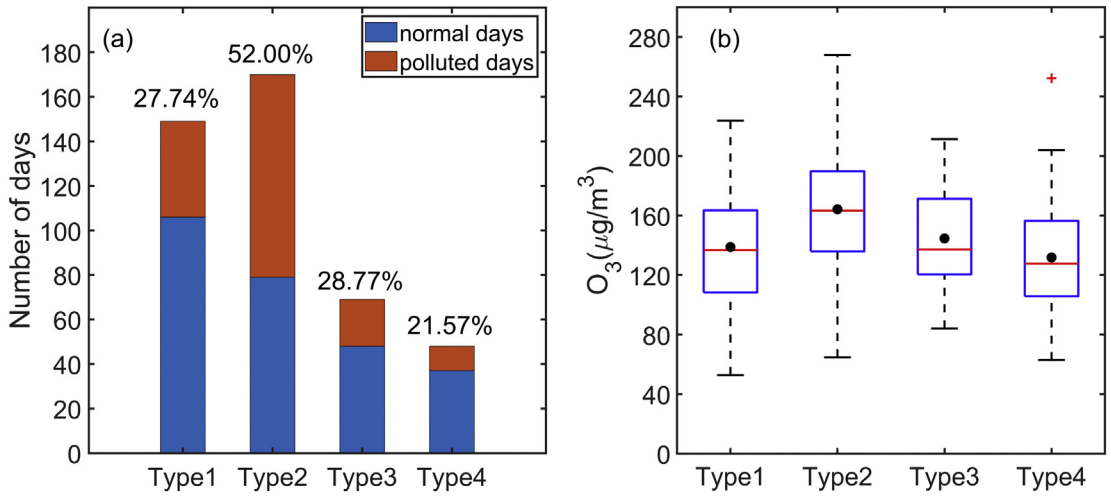

Fig. 5. a) Number of normal days (defined as the days of MDA8 < 160 μg/m^3) and ozone polluted days (defined as the days of MDA8 ≥160 μg/m^3) in each type, the percentage above each bar represents the frequency of ozone polluted days for synoptic type; b) Boxplot of MDA8 ozone concentration of each synoptic type. The red "+" marks the outlier. The central red line indicates the median, and the black dot represents the mean after removing the outliers. The bottom and top edges of the boxes are the 25th and the 75th percentiles, respectively. The whiskers extend from the minimum to the maximum values. (For interpretation of the references to colour in this figure legend, the reader is referred to the web version of this article.)

160°E by including Northwest Pacific. Type 2 shows the highest frequency of occurrence, accounting for 38.55% of all days. It represents a low pressure anomaly in the northwest and a positive anomaly over Northwest Pacific Ocean to the east of the NCP, which is controlled by a weak low pressure system. Type 1 occurs on 34.14% of summer days and ranks only second to Type 2. It shows a generally reversed pattern to Type 2, with high pressure center to the northwest, and low SLP anomalies over the oceans to the east. The NCP region is at the edge of the northwest high pressure anomaly. Type 3 and Type 4 account for 16.08% and 11.23% of the days respectively. In Type 3, NCP is under the control of a high pressure center extending from Northeast China to the South NCP area, whereas for Type 4, NCP is mostly influenced by a low pressure system in the south.

3.3. Relationship between synoptic pattern and ozone pollution

Next, we examine the surface ozone concentration in the NCP associated with the four synoptic patterns. Fig. 5 presents the corresponding frequencies of ozone pollution (MDA8 exceeding 160 $\mu g/m^3$) occurrences and box-whisker plots of MDA8 ozone concentrations for the four patterns. Type 2 clearly stands out with the highest mean (~164$\mu g/m^3$) and maximum (exceeding 265$\mu g/m^3$) MDA8 ozone concentrations. More than half (52%) of days in Type 2 are associated with ozone pollution. Type1 and Type3 have the similar frequencies of ozone pollution occurrences, which are 27.74% and 28.78% respectively. Their averaged ozone concentrations are also comparable. The lowest mean MDA8 ozone concentration (~132$\mu g/m^3$) is found for Type 4, which also has the lowest frequency of ozone pollution occurrences (21.57%). The spatial distributions of MDA8 ozone concentration in the NCP and surrounding area under the four patterns also show great differences across the four types as demonstrated by Fig. 6. Typically, higher ozone concentration is found in Beijing, Tianjin, the South of Hebei province and the West of Shandong province. Mean ozone concentration for Type 2 greatly exceeds that for the other three types by as much 50%.

The change of ozone pollution under different synoptic patterns should be primarily attributed to the changes of local meteorological variables, which impact on the photochemical reaction processes as well as dispersion/removal processes. Therefore, in Fig. 7, we examine the anomalies of key meteorological variables, including temperature, relative and specific humidity, horizontal winds, cloud cover, surface downward UV radiation and precipitation. For Type 2 that has the highest surface ozone concentration, a clear warm anomaly as large as 1.5 °C is observed over the NCP. The RH is slightly decreased by ~3%, whereas specific humidity shows positive anomalies in the northeast NCP around Beijing and negative anomalies elsewhere. The wind field shows southwest anomalies which are caused by a positive SLP anomaly center to the east of this area. These winds bring warm, dry air from inland South China to the south of NCP and result in the high temperature, low RH condition there. For the north of NCP, the southwest winds may also pass by the oceans and carry moisture, causing an increase of specific humidity. However, since temperature also increases, the resulting RH shows a neutral change. Consistent with the moisture change, cloud cover as well as precipitation decreases and surface UV radiation

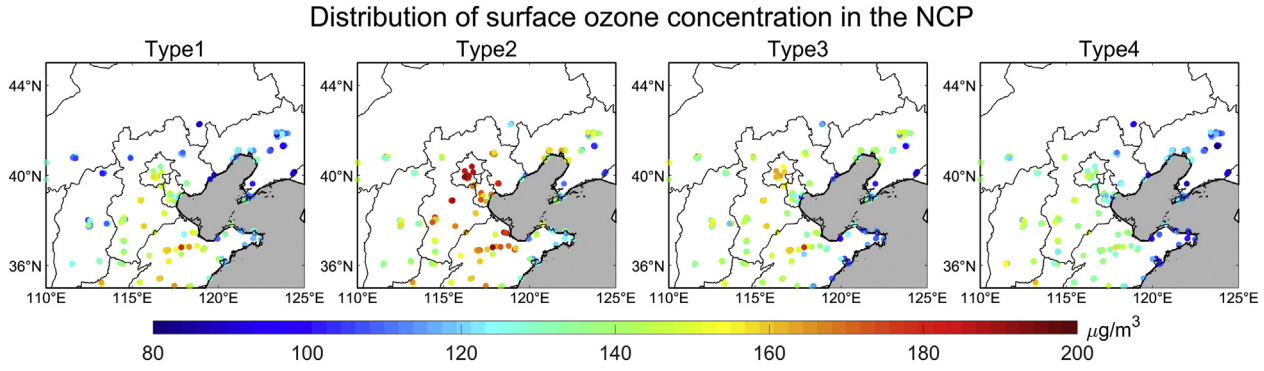

Fig. 6. Distribution of surface ozone concentration in the NCP for each synoptic type.

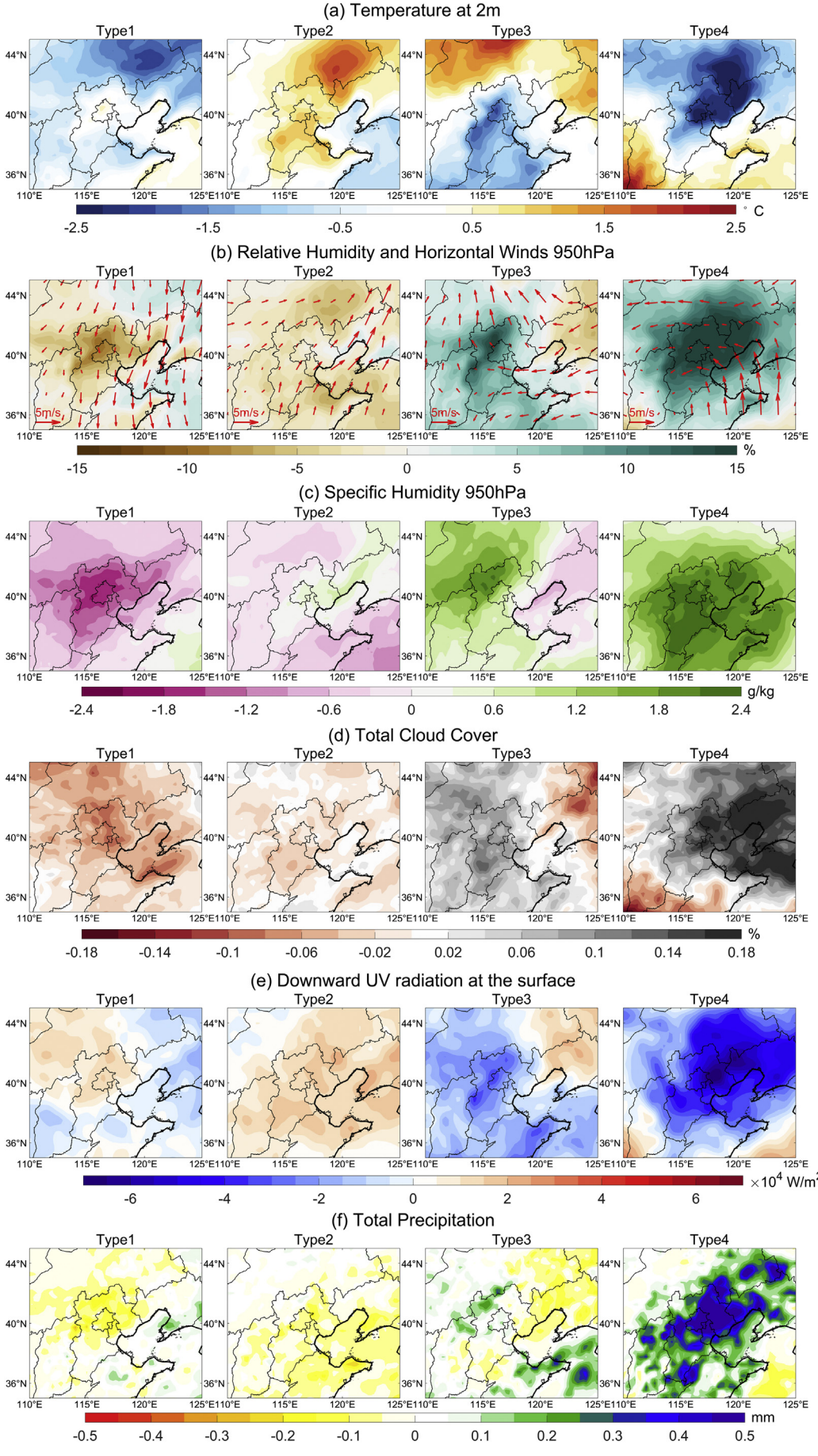
(a) Temperature at 2m
Type1
Type2
Type3
Type4
44°N
40°N
36°N
110°E
115°E
120°E
125°E
°C
-2.5
-1.5
-0.5
0.5
1.5
2.5
(b) Relative Humidity and Horizontal Winds 950hPa
5m/s
%
-15
-10
-5
0
5
10
15
(c) Specific Humidity 950hPa
g/kg
-2.4
-1.8
-1.2
-0.6
0
0.6
1.2
1.8
2.4
(d) Total Cloud Cover
%
-0.18
-0.14
-0.1
-0.06
-0.02
0.02
0.06
0.1
0.14
0.18
(e) Downward UV radiation at the surface
×10^4 W/m^2
-6
-4
-2
0
2
4
6
(f) Total Precipitation
mm
-0.5
-0.4
-0.3
-0.2
-0.1
0
0.1
0.2
0.3
0.4
0.5

increases. The enhanced temperature and UV increases surface ozone production by two principal mechanisms (Sillman and Samson, 1995; Jacob and Winner, 2009; Doherty et al., 2013): (1) enhancing the photolysis rate of NO_x via accelerating the thermal decomposition of proxyacetylnitrate (PAN, a major NO_x reservoir species); and (2) favoring the temperature-dependent biogenic emission of isoprene (a major VOC precursor of photochemical reaction under high-NO_x conditions). The role of RH on ozone formation is more complicated for different regimes of water vapor (HO_x sources) under different conditions, as RH is a proxy of HO_x ($HO_x = OH + H +$ peroxy radicals) concentration (Jacob and Winner, 2009; Lu et al., 2019b). In the regions with low-NO_x levels, increasing RH decreases ozone concentration significantly by the reaction (Johnson et al., 1999):

$$O_3 + h\nu \rightarrow O_2 + O(^1D) \#(R1)$$

$$O(^1D) + H_2O \rightarrow 2OH \#(R2)$$

where (*R2*) competes with the oxidizing reaction of $O(^1D)$ with N_2 or O_2. In addition, over the polluted regions with high-NO_x levels, the OH radicals produced by (*R2*) can affect the photochemical reaction by (1) reacting with VOCs and CO which raises ozone production and (2) converting NO_2 to nitric acid which suppresses ozone formation (Jacob and Winner, 2009; Lu et al., 2019b). Thus, various relationships with different signs have been reported globally (Baertsch-Ritter et al., 2004; Camalier et al., 2007; Doherty et al., 2013). Precipitation primarily serves to reduce ozone through wet deposition (Meleux et al., 2007; Dawson et al., 2007), although the counteracting effect by reduced aerosol and NO_x may compensate for some ozone loss, mainly over VOC-limited regions (Wang et al., 2019). In addition, clouds can hamper ozone production and expedite ozone elimination via affecting photochemical reaction and aqueous-phase chemistry (Lelieveld and Crutzen, 1990). In short, higher temperature, lower RH, precipitation and cloud fraction all contribute positively to surface ozone concentration and lead to its positive anomaly for Type 2.

In contrast, Type 4 has the lowest level of ozone pollution, where a strong reversed pattern to that of Type 2 is observed. This type is associated with a low pressure center to the west of NCP. The surface air flow thus exhibits a cyclonic pattern, with southerly and southeast winds blowing from the oceans over most of the NCP. These cool and humid air masses result in the low temperature, high RH, cloud cover, precipitation and low UV radiation environment. According to the above discussion, all these conditions are unfavorable to the production of surface ozone. The anomaly patterns for Type 3 is like a weaker version of Type 4, except that the surface winds follow an anticyclonic pattern caused by the high pressure center over the northeast of NCP. The east winds from the oceans also cool the surface and increase the moisture content. However, the magnitude of the wind anomalies is only about half of that under Type 4, and thus the meteorological changes are also weaker. These changes are also unfavorable for the production of surface ozone and result in the relative low ozone concentration.

Finally, it is worth noting that the signs of temperature, radiation and moisture changes for Type 1 are similar to those of Type 2, yet it is associated with significantly lower ozone pollution level. The major difference lies in the surface wind pattern. In Type 1 strong northerly wind anomalies are observed corresponding to the weakened WPSH and high SLP anomaly in the northwest (Fig. 8), which is opposite to the prevailing wind direction in Type 2. These northerly winds enhance the dispersion and transport of pollutants in spite of its favorable photochemical conditions. On the contrary, the southerly winds in Type 2 tend to result in the accumulation of pollutants in the NCP due to the blocking effect by the mountain ranges to the north and the west. The difference in surface ozone concentration between Type 1 and Type 2 highlights the importance of regional transport in the formation of heavy pollution events.

Meteorological variables including temperature, moisture conditions, radiation, precipitation and cloud cover affect ozone pollution by contributing to local photochemical reaction rates. Surface ozone concentration, on the other hand, also depends on regional transport, in which the movements of air mass play critical roles. In Fig. 8, we compare the footprints of backward trajectories for each synoptic pattern as a proxy of regional ozone transportation. For Type 2, which has the highest ozone concentration, the air masses mainly come from the south, including Shandong, Henan, Jiangsu Provinces and the Shanghai City. Evident from Fig. 1, these places have heavy ozone pollution during the summer, implying that regional transport may contribute to the aggravation of ozone pollution in the NCP. Sustained northerly winds appear in Type1 which bring clean fresh air from far north and help clean up local pollution, resulting in lower surface ozone concentrations. As for Types 3 and 4, clean flows via the ocean contribute to low concentrations in coastal areas, although the ranges of transport for these two types are relatively small compared to the other two types.

3.4. Relationship between PBLH and ozone pollution under different synoptic patterns

In addition to the local photochemical reaction and regional horizontal transport, the vertical dispersion is another critical factor controlling surface ozone concentration. This process mainly happens in the PBL and the total volume of vertical dispersion depends on the PBLH. For this reason, in this section we focus on the relationship between the PBLH and ozone pollution for different circulation patterns.

The averaged PBLH calculated using radiosonde data for the four types are shown in Fig. 9a. We note that Type 4 which has the lowest overall ozone concentration also shows the lowest PBLH. However, for Type 2 with the highest ozone concentration, the PBLH ranks the second highest and does not stand out. This implies a non-linear relationship between PBLH and ozone pollution. We therefore further examine the ozone concentration under different PBLH ranges in Fig. 9b. Expectedly, the change of surface ozone concentration with PBLH indeed follows a non-linear behavior, i.e., it first increases with PBLH till ~PBLH = 0.9 km, then remains stable till ~PBLH = 1.5 km, and starts to decline as PBLH further increases. The mechanism that PBLH impacts on surface ozone pollution may involve several chemical and physical processes. First, higher PBLH corresponds to more active mixing between the surface and upper-level atmosphere. Because ozone concentration is typically higher near the top of PBL and all the way to the free troposphere than at the surface due to stronger solar radiation and the accumulation of ozone precursors near the boundary layer top, enhanced mixing induces stronger downward transport of ozone to the surface (Sun et al., 2010). Second, low primary pollutant concentration (except for NO_2 due to its short lifetime) at surface resulting from the intensive vertical dispersion under high PBLH may also contribute to a positive relationship between ozone and PBLH because of complicated mechanisms, i.e., low PM concentration can increase ozone concentrations by slowing down the aerosol sink of hydroperoxy (HO_2) radicals and accelerating ozone production (Li et al., 2019), and low sulfur dioxide (SO_2) decreases sulfate and thus enhances ozone production through aerosol effects (Liu and Wang, 2020; He et al., 2017). The third one is the physical process that higher PBLH leads to increased vertical dispersion of surface ozone and serves to decrease pollution level due to the well-established positive air pollutant–PBL feedback (Dawson et al., 2007; Su et al., 2018). We hypothesize that the behavior in Fig. 9 is likely the combined effect of these three mechanisms mentioned above. When PBLH is lower than 0.9 km, the first two mechanisms dominate and ozone concentration tends to increase with PBLH.

Fig. 7. Averaged anomalies for a) 2 m temperature; b) 950 hPa relative humidity and horizontal wind fields; c) 950 hPa specific humidity; d) total cloud cover; e) downward UV radiation at the surface and f) total precipitation, for each circulation type.

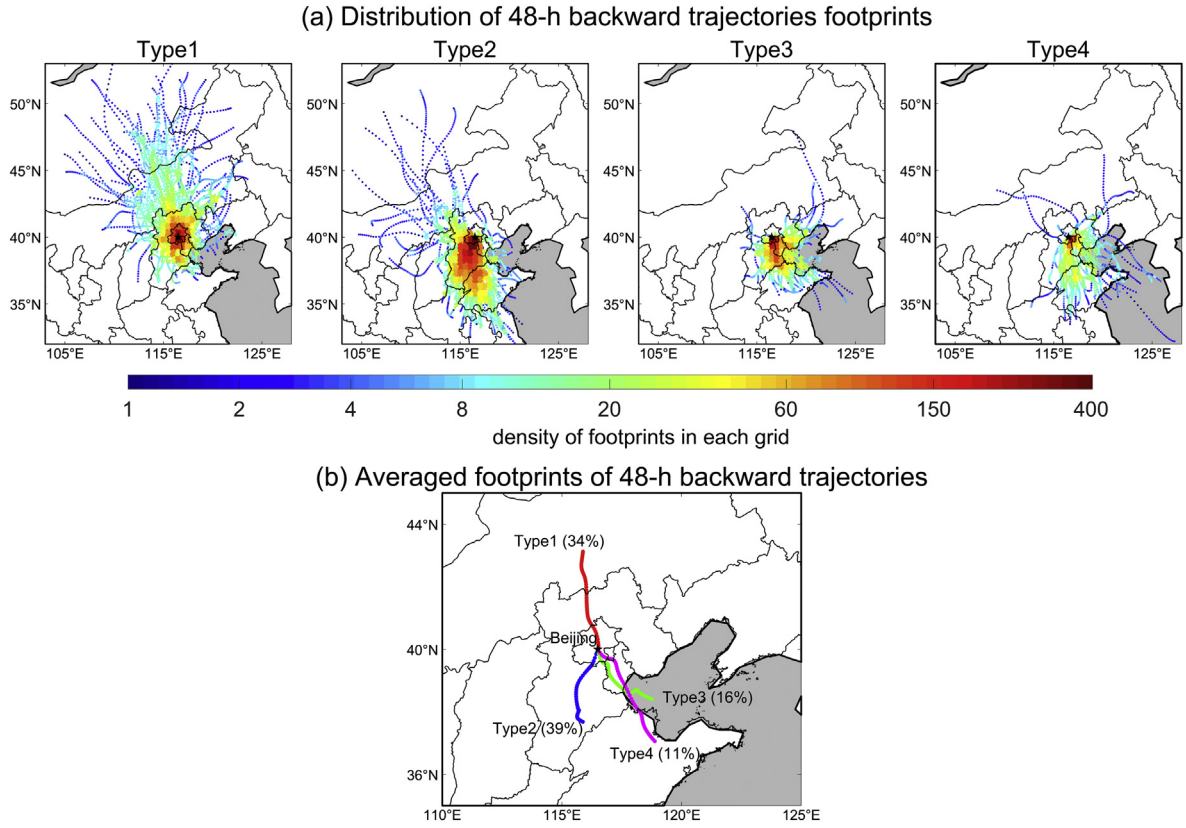

Fig. 8. a) Density distribution of 48-h backward trajectories for each synoptic pattern, where the density of footprints refers to the number of hourly footprints in each grid (0.5° × 0.5°); b) Averaged 48-h backward trajectories for the four synoptic patterns.

Between 0.9 km and 1.5 km PBLH, the strengths of the first two effects and the third effect are competing, i.e., upward dispersion matches downward transport so that ozone level remains constant. When PBLH is higher than 1.5 km, the third effect dominates and thus the surface ozone concentration is observed to decrease. However, substantial observations and modeling are needed to fully clarify the mechanism, and we intend to leave that for a future study.

The development of the PBL critically depends on the temperature structure and the thermal stratification in the lower atmosphere. We thus further compare the potential temperature profiles across the four synoptic types in Fig. 10, to gain some insights into the possible causes of their different PBLHs. Both Type 1 and Type 2 exhibit warm anomalies within the PBL, whereas distinct cold anomalies are observed in Types 3 and 4. The warm anomaly in Type 1 quickly shifts to strong cold anomaly near the PBL top. The warm anomaly of Type 2 is stronger and more consistent within the PBL, indicating better mixing. The potential temperature anomalies of these two types both promote the development of the PBL by weakening the thermal inversion at the PBL top, which benefits the downward transport from upper levels where ozone concentrations are usually higher than that at the surface (Sun et al., 2010; Gong and Liao, 2019). Moreover, the higher surface ozone concentration in Type 2 than in Type 1 is likely related to the higher local photochemical production of ozone and additional transport from the south. In contrast, the potential temperature anomalies of

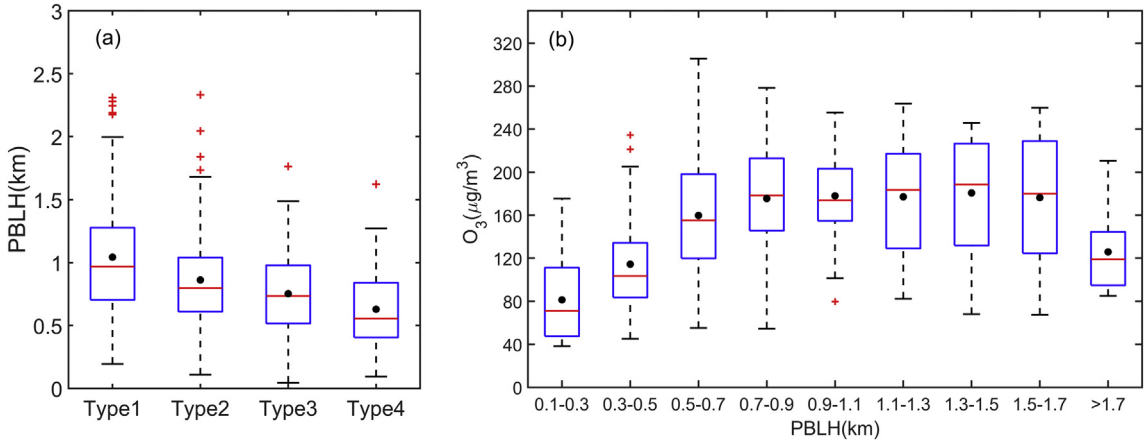

Fig. 9. a) The boxplots of planetary boundary layer height (PBLH) calculated using the additional sounding data at 14:00 BJT for four circulation types; b) The variability of MDA8 ozone concentration with PBLH. The red "+" marks the outlier. The central red line indicates the median, and the black dot represents the mean after removing the outliers. The bottom and top edges of the boxes are the 25th and the 75th percentiles, respectively. The whiskers extend from the minimum to the maximum values. (For interpretation of the references to colour in this figure legend, the reader is referred to the web version of this article.)

the Types 3 and 4 tend to enhance the thermal inversion at the PBL top, suppressing the development of the PBL and reducing its height. The virtual temperature gradient is stronger in Type 4 than that in Type 3, with the cold anomaly shifting to warm anomaly above the PBL, leading to stronger inversion and lower PBL. For both these two types, ozone concentration near surface is limited due to the cold temperature and weak vertical mixing. Note that due to the development of PBL structure, the effects of the above three mechanisms may vary with hour, which indicate that the relationship between ozone and PBLH may be associate with the diurnal variability of PBLH. For example, the downward transport from upper levels listed as the first reason is strong before the noon (Sun et al., 2010), whereas the third effect (vertical dispersion) lasts the entire daytime (Miao et al., 2015). However, because radiosonde measurements are only performed at limited times of the day, we cannot obtain a full PBLH diurnal cycle, making it difficult to thoroughly investigate the ozone-PBLH relationship. In the future, we will try to fill this gap by seeking other data sources and conducting model simulations.

4. Discussion

From what we have investigated above, close relationship between synoptic patterns and ozone pollution is confirmed. Unlike the above-mentioned studies, we demonstrate a long-time ground-level ozone variability under different synoptic patterns in NCP region. Ozone pollution events usually occur with a positive anomaly over the Northwest Pacific as found in our study as Type 2. Zhang et al. (2016) indicated summer pollution in the NCP region often occurred when a low pressure system was centered in the north of the NCP, located at the west edge of high pressure system. Yin et al. (2019a, 2019b) also found that surface ozone variability in North China was partly driven by the Arctic sea ice via the summer west Pacific pattern. These patterns both show

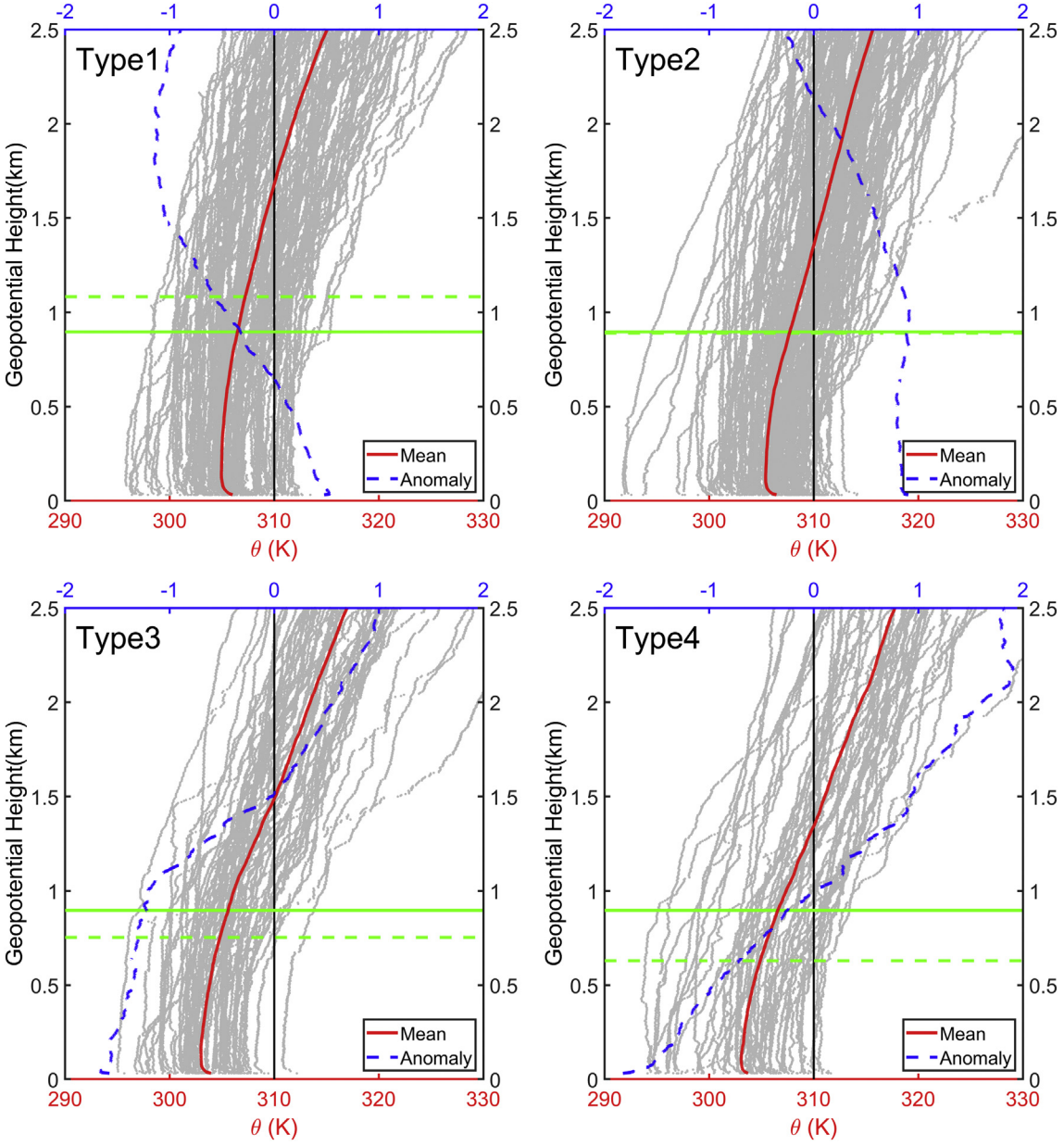

Fig. 10. Vertical profiles of potential temperature (θ) at 1400 BJT for each synoptic type. Red lines indicate averaged θ profile for the four types, and blue dashed lines represent the θ anomaly (subtracted from the mean values of summer θ profiles). All daily θ profiles for each synoptic type are plotted as thin gray lines. The Green solid lines indicate the averaged PBLH in summer, and the green dashed lines mark the averaged PBLH for each synoptic type. (For interpretation of the references to colour in this figure legend, the reader is referred to the web version of this article.)

similar circulation variabilities as our Type 2. The meteorological conditions with high ozone concentration in Type 2 are consistent with previous studies, including high temperature, moderate humidity, low cloud coverage, much radiation and southerly winds (Wang et al., 2017; Doherty et al., 2013; Lu et al., 2019b). We further reveal a non-linear relationship between ozone and PBLHs as well as their corresponding PBL structures under various synoptic pattern classifications. The analysis of synoptic patterns and related meteorological variables serve to explain high ozone pollution in NCP associated with positive net photochemical production, horizontal transport and vertical advection (Gong and Liao, 2019; Lu et al., 2019a) under the drivers of large circulations such as EU via positive west Pacific summer high pressure systems (Yin et al., 2019a). As such, we argue that more attention could be drawn to those high occurrences of ozone pollution events when the Northwest Pacific SLP shows positive anomalies and a lower pressure system centers in the north of NCP region.

Moreover, an increasing trend in surface ozone concentration over East China has been observed for the past five years. Reduced PM and NO_x emission is considered to be the primary driver of this trend (Li et al., 2019). Here, we also briefly discuss whether the change in meteorology is related to the ozone trend. As seen from Fig. 11a, the NCP region has been experiencing an aggravated ozone pollution in past five years, especially during 2017 and 2018. However, the frequency of occurrence of Type 2 synoptic pattern does not increase but shows a nearly consistent year-to-year declining tendency in Fig. 11b. This implies that meteorology is unlikely a cause of the observed ozone increase, which further supports the conclusion by previous studies on emission changes (Li et al., 2019; Wang et al., 2019; Liu and Wang, 2020).

5. Conclusions

In this study, we investigate the relationship between synoptic pattern and surface ozone pollution in the North China Plain region. The associated changes of meteorological variables for different synoptic patterns are analyzed to examine the possible mechanism for the ozone changes, with a more detailed discussion on the impact of the boundary layer. Our main conclusions are summarized below:

1) Four prevailing synoptic patterns in the summer are identified over the NCP. Types 1 and 2 show mostly reversed patterns with negative and positive anomalies over the Northwest Pacific respectively, with high (Type 1) or low (Type 2) pressure centers to the northwest. Type 3 represents the control of a high pressure system extending from Northeast China to the South of NCP area, whereas in Type 4, a low pressure system appears in the south of NCP.
2) The highest surface ozone concentration is observed in the Type 2 pattern. The meteorological conditions for this type are characterized by high temperature, low humidity that favor the chemical production of surface ozone, and southerly flows which contribute to the transport of ozone and its precursors to the NCP region.
3) The relationship between PBLH and surface ozone concentration is non-linear. Surface ozone concentration initially increases with PBLH till ~PBLH = 0.9 km, remains stable till ~PBLH = 1.5 km, and decreases as PBLH further increases. This may reflect the reconciling effect between enhanced downward ozone transport and stronger vertical dispersion as PBLH increases. Strong warm anomalies within the PBL occur in Type 2 which contributes to its higher ozone concentration.
4) Meteorological factors are unlikely responsible for the observed ozone increase over the NCP from 2014 to 2018, because the frequency of Type 2 shows a declining tendency.

So far our work has related synoptic patterns to ozone variability through statistical analysis. In the future, we will continue to investigate the mechanism with model simulations to clarify the key chemical and physical processes that lead to increased ozone production. In particular, we will conduct sensitivity experiments to test our hypothesis about PBLH-ozone relationship. Other pollution hotspots such as the Yangtze River Delta and Pearl River Delta of China will also be our future focus, with the goal of identifying both the common and unique synoptic features associated with ozone pollution in megacities of China.

CRediT authorship contribution statement

Yueming Dong: Investigation, Methodology, Writing - original draft. **Jing Li:** Conceptualization, Supervision, Writing - original draft, Funding acquisition. **Jianping Guo:** Resources, Data curation, Writing - review & editing. **Zhongjing Jiang:** Investigation, Data curation. **Yiqi Chu:** Methodology. **Liang Chang:** Software. **Yang Yang:** Funding acquisition, Writing - review & editing. **Hong Liao:** Funding acquisition, Writing - review & editing.

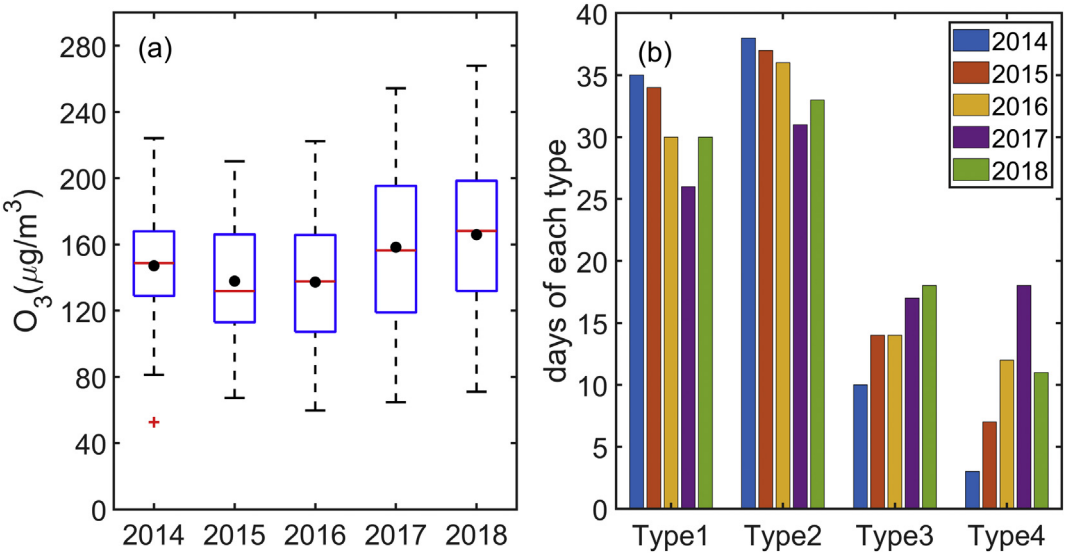

Fig. 11. a) Summertime ozone variability in from 2014 to 2018. The red "+" marks the outlier. The central red line indicates the median, and the black dot represents the mean after removing the outliers. The bottom and top edges of the boxes are the 25th and the 75th percentiles, respectively. The whiskers extend from the minimum to the maximum values; b) The number of each synoptic type for the summers of 2014 to 2018. (For interpretation of the references to colour in this figure legend, the reader is referred to the web version of this article.)

Declaration of competing interest

The authors declare that they have no known competing financial interests or personal relationships that could have appeared to influence the work reported in this paper.

Acknowledgements

We thank the China National Environmental Monitoring Centre for supporting the nationwide ozone monitoring network and the website (http://beijingair.sinaapp.com/) for collecting and sharing hourly ozone concentration data. We appreciate CMA for providing the long-term sounding data, and ECMWF for providing hourly ERA5 reanalysis data in our work. We also acknowledge the efforts of NOAA ARL working groups for developing and managing the HYSPLIT model, and the cost733class software for supporting T-PCA classification. This work is funded by National Key Research and Development Program of China (Nos. 2017YFC0212803, 2017YFC1501401) and Open fund by Jiangsu Key Laboratory of Atmospheric Environment Monitoring and Pollution Control (KHK1901).

References

Baertsch-Ritter, N., Keller, J., Dommen, J., Prevot, A.S.H., 2004. Effects of various meteorological conditions and spatial emissionresolutions on the ozone concentration and ROG/NO_x limitationin the Milan area (I). Atmos. Chem. Phys. 4, 423–438. https://doi.org/10.5194/acp-4-423-2004.

Benjamini, Y., Hochberg, Y., 1995. Controlling the false discovery rate: a practical and powerful approach to multiple testing. J. Roy. Stat. Soc., B 57, 289–300.

Bloomer, B.J., Stehr, J.W., Piety, C.A., Salawitch, R.J., Dickerson, R.R., 2009. Observed relationships of ozone air pollution with temperature and emissions. Geophys. Res. Lett. 36, 269–277.

Camalier, L., Cox, W., Dolwick, P., 2007. The effects of meteorology on ozone in urban areas and their use in assessing ozone trends. Atmos. Environ. 41, 7127–7137.

Chan, C.K., Yao, X., 2008. Air pollution in mega cities in China. Atmos. Environ. 42, 1–42. https://doi.org/10.1016/j.atmosenv.2007.09.003.

Chen, D., Guo, J., Yao, D., Lin, Y., Zhao, C., Min, M., Xu, H., Liu, L., Huang, X., Chen, T., Zhai, P., 2019. Mesoscale convective systems in East Asia from advanced Himawari imager: algorithms and preliminary results. J. Geophys. Res. Atmos. 124, 2210–2234. https://doi.org/10.1029/2018JD029707.

Chen, H., Wang, H., 2015. Haze days in North China and the associated atmospheric circulations based on daily visibility data from 1960 to 2012. J. Geophys. Res. Atmos. 120, 5895–5909.

Cheng, W.L., Pai, J.L., Tsuang, B.J., Chen, C.L., 2001. Synoptic patterns in relation to ozone concentrations in West-Central Taiwan. Meteorog. Atmos. Phys. 78, 11–21.

Comrie, A.C., Yarnal, B., 1992. Relationships between synoptic-scale atmospheric circulation and ozone concentrations in metropolitan Pittsburgh, Pennsylvania. Atmos. Environ. 26, 301–312.

Copernicus Climate Change Service (C3S), 2017. ERA5: Fifth Generation of ECMWF Atmospheric Reanalyses of the Global Climate. Copernicus Climate Change Service Climate Data Store (CDS) https://cds.climate.copernicus.eu/cdsapp#!/home.

Davis, R.E., Normile, C.P., Sitka, L., Hondula, D.M., Knight, D.B., Gawtry, S.P., Stenger, P.J., 2010. A comparison of trajectory and air mass approaches to examine ozone variability. Atmos. Environ. 44, 64–74.

Dawson, J.P., Adams, P.J., Pandis, S.N., 2007. Sensitivity of ozone to summertime climate in the eastern USA: a modeling case study. Atmos. Environ. 41, 1494–1511.

Dayan, U., Levy, I., 2002. Relationship between synoptic-scale atmospheric circulation and ozone concentrations over Israel. J. Geophys. Res. Atmos. 107, 4813. https://doi.org/10.1029/2002JD002147.

Demuzere, M., Trigo, R.M., Vila-Guerau de Arellano, J., van Lipzig, N.P.M., 2009. The impact of weather and atmospheric circulation on O_3 and PM_{10} levels at a rural mid-latitude site. Atmos. Chem. Phys. 9, 2695–2714. https://doi.org/10.5194/acp-9-2695-2009.

Ding, A.J., Wang, T., Thouret, V., Cammas, J.-P., Nédélec, P., 2008. Tropospheric ozone climatology over Beijing: analysis of aircraft data from the MOZAIC program. Atmos. Chem. Phys. 8, 1–13. https://doi.org/10.5194/acp-8-1-2008.

Ding, A.J., Wang, T., Xue, L.K., Gao, J., Stohl, A., Lei, H.C., Jin, D.Z., Ren, Y., Wang, X.Z., Wei, X.L., Qi, Y.B., Liu, J., Zhang, X.Q., 2009. Transport of north China air pollution by mid-latitude cyclones: case study of aircraft measurements in summer 2007. J. Geophys. Res. 114, D08304. https://doi.org/10.1029/2008JD011023.

Ding, A.J., Fu, C.B., Yang, X.Q., Sun, J.N., Zheng, L.F., Xie, Y.N., Herrmann, E., Nie, W., Petäjä, T., Kerminen, V.-M., Kulmala, M., 2013. Ozone and fine particle in the western Yangtze River Delta: an overview of 1 yr data at the SORPES station. Atmos. Chem. Phys. 13, 5813–5830. https://doi.org/10.5194/acp-13-5813-2013.

Ding, Y., 1992. Summer monsoon rainfalls in China. J. Meteor. Soc. Japan. Ser. II 70 (1B), 373–396.

Doherty, R.M., Wild, O., Shindell, D.T., Zeng, G., MacKenzie, I.A., Collins, W.J., Fiore, A.M., Stevenson, D.S., Dentener, F.J., Schultz, M.G., Hess, P., Derwent, R.G., Keating, T.J., 2013. Impacts of climate change on surface ozone and intercontinental ozone pollution: a multi-model study. J. Geophys. Res. 118, 3744–3763. https://doi.org/10.1002/jgrd.50266.

Draxler, R.R., Hess, G.D., 1998. An overview of the HYSPLIT4 modeling system for trajectories, dispersion, and deposition. Aust. Meteor. Mag. 47, 295–308.

Gao, J., Wang, T., Ding, A.J., Liu, C.B., 2005. Observational study of ozone and carbon monoxide at the summit of mount Tai (1534 m a.s.l.) in central-eastern China. Atmos. Environ. 39, 4779–4791.

Gao, Y., Liu, X., Zhao, C., Zhang, M., 2011. Emission controls versus meteorological conditions in determining aerosol concentrations in Beijing during the 2008 Olympic games. Atmos. Chem. Phys. 11, 12437–12451. https://doi.org/10.5194/acp-11-12437-2011.

Gong, C., Liao, H., 2019. A typical weather pattern for ozone pollution events in North China. Atmos. Chem. Phys. 19, 13725–13740. https://doi.org/10.5194/acp-19-13725-2019.

Goodman, J.E., Prueitt, R.L., Sax, S.N., Pizzurro, D.M., Lynch, H.N., Zu, K., Venditti, F.J., 2015. Ozone exposure and systemic biomarkers: evaluation of evidence for adverse cardiovascular health impacts. Crit. Rev. Toxicol. 45 (5), 412–452. https://doi.org/10.3109/10408444.2015.1031371.

Guo, J., Miao, Y., Zhang, Y., Liu, H., Li, Z., Zhang, W., He, J., Lou, M., Yan, Y., Bian, L., Zhai, P., 2016. The climatology of planetary boundary layer height in China derived from radiosonde and reanalysis data. Atmos. Chem. Phys. 16, 13309–13319. https://doi.org/10.5194/acp-16-13309-2016.

He, J., Gong, S., Yu, Y., Yu, L., Wu, L., Mao, H., Song, C., Zhao, S., Liu, H., Li, X., Li, R., 2017. Air pollution characteristics and their relation to meteorological conditions during 2014–2015 in major Chinese cities. Environ. Pollut. 223, 484–496. https://doi.org/10.1016/j.envpol.2017.01.050.

He, J., Gong, S., Zhou, C., Lu, S., Wu, L., Chen, Y., Yu, Y., Zhao, S., Yu, L., Yin, C., 2018. Analyses of winter circulation types and their impacts on haze pollution in Beijing. Atmos. Environ. 192, 94–103. https://doi.org/10.1016/j.atmosenv.2018.08.060.

Hegarty, J., Mao, H., Talbot, R., 2007. Synoptic controls on summertime surface ozone in the northeastern United States. J. Geophys. Res. 112, D14306. https://doi.org/10.1029/2006jd008170.

Hegarty, J., Mao, H., Talbot, R., 2009. Synoptic influences on springtime tropospheric O_3 and CO over the north American export region observed by TES. Atmos. Chem. Phys. 9, 3755–3776. https://doi.org/10.5194/acp-9-3755-2009.

Huth, R., Beck, C., Philipp, A., Demuzere, M., Ustrnul, Z., Cahynová, M., Kyselý, J., Tveito, O.E., 2008. Classifications of atmospheric circulation patterns: recent advances and applications. Ann. N. Y. Acad. Sci. 1146, 105–152. https://doi.org/10.1196/annals.1446.019.

Jacob, D.J., Winner, D.A., 2009. Effect of climate change on air quality. Atmos. Environ. 43, 51–63. https://doi.org/10.1016/j.atmosenv.2008.09.051.

Jiang, Y.C., Zhao, T.L., Liu, J., Xu, X.D., Tan, C.H., Cheng, X.H., Bi, X.Y., Gan, J.B., You, J.F., Zhao, S.Z., 2015. Why does surface ozone peak before a typhoon landing in Southeast China? Atmos. Chem. Phys. 15, 13331–13338. https://doi.org/10.5194/acp-15-13331-2015.

Johnson, C.E., Collins, W.J., Stevenson, D.S., Derwent, R.G., 1999. The relative roles of climate and emissions changes on future oxidant concentrations. J. Geophys. Res. 104, 18,631–18,645.

Johnson, N.C., 2012. How many ENSO flavors can we distinguish? J. Clim. 26, 4816–4827.

Lelieveld, J., Crutzen, P.J., 1990. Influences of cloud photochemical processes on tropospheric ozone. Nature 343, 227–233. https://doi.org/10.1038/343227a0.

Li, K., Jacob, D.J., Liao, H., Shen, L., Zhang, Q., Bates, K.H., 2019. Anthropogenic drivers of 2013–2017 trends in summer surface ozone in China. P. Natl. Acad. Sci. USA 116, 422–427. https://doi.org/10.1073/pnas.1812168116.

Li, Z., Guo, J., Ding, A., Liao, H., Liu, J., Sun, Y., Wang, T., Xue, H., Zhang, H., Zhu, B., 2017. Aerosol and boundary-layer interactions and impact on air quality. Natl. Sci. Rev. 4 (6), 810–833. https://doi.org/10.1093/nsr/nwx117.

Liu, J., Wang, L., Li, M., Liao, Z., Sun, Y., Song, T., Gao, W., Wang, Y., Li, Y., Ji, D., Hu, B., Kerminen, V.-M., Wang, Y., Kulmala, M., 2019a. Quantifying the impact of synoptic circulation patterns on ozone variability in northern China from April to October 2013–2017. Atmos. Chem. Phys. 19, 14477–14492. https://doi.org/10.5194/acp-19-14477-2019.

Liu, N., Zhou, S., Liu, C., Guo, J., 2019b. Synoptic circulation pattern and boundary layer structure associated with $PM_{2.5}$ during wintertime haze pollution episodes in Shanghai. Atmos. Res. 228, 186–195. https://doi.org/10.1016/j.atmosres.2019.06.001.

Liu, Y., Wang, T., 2020. Worsening urban ozone pollution in China from 2013 to 2017 – part 2: the effects of emission changes and implications for multi-pollutant control. Atmos. Chem. Phys. Discuss. https://doi.org/10.5194/acp-2020-53 review.

Lu, X., Zhang, L., Chen, Y., Zhou, M., Zheng, B., Li, K., Liu, Y., Lin, J., Fu, T.-M., Zhang, Q., 2019a. Exploring 2016–2017 surface ozone pollution over China: source contributions and meteorological influences. Atmos. Chem. Phys. 19, 8339–8361. https://doi.org/10.5194/acp-19-8339-2019.

Lu, X., Zhang, L., Shen, L., 2019b. Meteorology and climate influences on tropospheric ozone: a review of natural sources, chemistry, and transport patterns. Curr Pollut. Rep 5, 238–260. https://doi.org/10.1007/s40726-019-00118-3.

Meleux, F., Solmon, F., Giorgi, F., 2007. Increase in summer European ozone amounts due to climate change. Atmos. Environ. 41, 7577–7587. https://doi.org/10.1016/j.atmosenv.2007.05.048.

Miao, Y., Liu, S., Zheng, Y., Wang, S., Chen, B., Zheng, H., Zhao, J., 2015. Numerical study of the effects of local atmospheric circulations on a pollution event over Beijing–Tianjin–Hebei, China. J. Environ. Sci. 30, 9–20.

Miao, Y., Guo, J., Liu, S., Liu, H., Li, Z., Zhang, W., Zhai, P., 2017. Classification of summertime synoptic patterns in Beijing and their associations with boundary layer structure affecting aerosol pollution. Atmos. Chem. Phys. 17, 3097–3110. https://doi.org/10.5194/acp-17-3097-2017.

Mills, G., Pleijel, H., Malley, C.S., Sinha, B., Cooper, O.R., Schultz, M.G., Neufeld, H.S., Simpson, D., Sharps, K., Feng, Z., Gerosa, G., Harmens, H., Kobayashi, K., Saxena, P., Paoletti, E., Sinha, V., Xu, X., 2018. Tropospheric ozone assessment report: present-day tropospheric ozone distribution and trends relevant to vegetation. Elem. Sci. Anth. 6, 47. https://doi.org/10.1525/elementa.302.

Philipp, A., Bartholy, J., Beck, C., Erpicum, M., Esteban, P., Fettweis, X., Huth, R., James, P., Jourdain, S., Kreienkamp, F., Krennert, T., Lykoudis, S., Michalides, S.C., Pianko-Kluczynska, K., Post, P., Álvarez, D.R., Schiemann, R., Spekat, A., Tymvios, F.S., 2010. Cost733cat – a database of weather and circulation type classifications. Phys. Chem. Earth 35, 360–373. https://doi.org/10.1016/j.pce.2009.12.010.

Pope, R.J., Butt, E.W., Chipperfield, M.P., Doherty, R.M., Fenech, S., Schmidt, A., Arnold, S.R., Savage, N.H., 2016. The impact of synoptic weather on UK surface ozone and implications for premature mortality. Environ. Res. Lett. 11, 124004. https://doi.org/10.1088/1748-9326/11/12/124004.

Richman, M.B., 1981. Obliquely rotated principal components: an improved meteorological map typing technique? J. Appl. Meteorol. 20, 1145–1159. https://doi.org/10.1175/1520-0450(1981)020<1145:ORPCAI>2.0.CO;2.

Santurtún, A., González-Hidalgo, J.C., Sanchez-Lorenzo, A., Zarrabeitia, M.T., 2015. Surface ozone concentration trends and its relationship with weather types in Spain (2001−2010). Atmos. Environ. 101, 10–22.

Seidel, D.J., Zhang, Y., Beljaars, A., Golaz, J.-C., Jacobson, A.R., Medeiros, B., 2012. Climatology of the planetary boundary layer over the continental United States and Europe. J. Geophys. Res.-Atmos. 117, 1–15. https://doi.org/10.1029/2012JD018143.

Shen, L., Mickley, L.J., Tai, A.P.K., 2015. Influence of synoptic patterns on surface ozone variability over the eastern United States from 1980 to 2012. Atmos. Chem. Phys. 15, 10925–10938. https://doi.org/10.5194/acp-15-10925-2015.

Sillman, S., Samson, P.J., 1995. The impact of temperature on oxidant formation in urban, polluted rural and remote environments. J. Geophys. Res. 100, 11497–11508.

Stein, A.F., Draxler, R.R., Rolph, G.D., Stunder, B.J.B., Cohen, M.D., Ngan, F., 2015. NOAA's HYSPLIT atmospheric transport and dispersion modeling system. B. Am. Meteorol. Soc. 96, 2059–2077. https://doi.org/10.1175/BAMS-D-14-00110.1.

Su, T., Li, Z., Kahn, R., 2018. Relationships between the planetary boundary layer height and surface pollutants derived from lidar observations over China: regional pattern and influencing factors. Atmos. Chem. Phys. 18, 15921–15935. https://doi.org/10.5194/acp-18-15921-2018.

Sun, Y., Wang, Y., Zhang, C., 2010. Vertical observations and analysis of $PM_{2.5}$, O_3, and NO_x at Beijing and Tianjin from towers during summer and autumn 2006. Adv. Atmos. Sci. 27, 123. https://doi.org/10.1007/s00376-009-8154-z.

Vogelezang, D.H.P., Holtslag, A.A.M., 1996. Evaluation and model impacts of alternative boundary-layer height formulations. Bound.-Layer Meteorol. 81, 245–269. https://doi.org/10.1007/BF02430331.

Wang, L., Guan, H., He, J., 2006. The position variation of the West Pacific subtropical high and its possible mechanism. J. Trop. Meteorol. 12, 113–120.

Wang, N., Lyu, X.P., Deng, X.J., Huang, X., Jiang, F., Ding, A.J., 2019. Aggravating O_3 pollution due to NO_x emission control in eastern China. Sci. Total Environ. 677, 732–744. https://doi.org/10.1016/j.scitotenv.2019.04.388.

Wang, T., Cheung, V.T.F., Lam, K.S., Kok, G.L., Harris, J.M., 2001. The characteristics of ozone and related compounds in the boundary layer of the south China coast: temporal and vertical variations during autumn season. Atmos. Environ. 35, 2735–2746.

Wang, T., Xue, L.K., Brimblecombe, P., Lam, Y.F., Li, L., Zhang, L., 2017. Ozone pollution in China: a review of concentrations, meteorological influences, chemical precursors, and effects. Sci. Total Environ. 575, 1582–1596. https://doi.org/10.1016/j.scitotenv.2016.10.081.

Wilks, D.S., 2006. On "field significance" and the false discovery rate. J. Appl. Meteorol. Climatol. 45, 1181–1189.

Xue, L.K., Wang, T., Louie, P.K.K., Luk, C.W.Y., Blake, D.R., Xu, Z., 2014. Increasing external effects negate local efforts to control ozone air pollution: a case study of Hong Kong and implications for other Chinese cities. Environ. Sci. Technol. 48, 10769–10775.

Yang, Y., Liao, H., Li, J., 2014. Impacts of the east Asian summer monsoon on interannual variations of summertime surface-layer ozone concentrations over China. Atmos. Chem. Phys. 14, 6867–6879. https://doi.org/10.5194/acp-14-6867-2014.

Yin, Z., Cao, B., Wang, H., 2019a. Dominant patterns of summer ozone pollution in eastern China and associated atmospheric circulations. Atmos. Chem. Phys. 19, 13933–13943. https://doi.org/10.5194/acp-19-13933-2019.

Yin, Z., Yuan, D., Zhang, X., Yang, Q., Xia, S., 2020. Different contributions of Arctic Sea ice anomalies from different regions to North China summer ozone pollution. Int. J. Climatol. 40, 559–571.

Yin, Z.C., Wang, H.J., Li, Y.Y., Ma, X.H., Zhang, X.Y., 2019b. Links of climate variability among Arctic sea ice, Eurasian teleconnection pattern and summer surface ozone pollution in North China. Atmos. Chem. Phys. 19, 3857–3871. https://doi.org/10.5194/acp-19-3857-2019.

Zhang, J.P., Zhu, T., Zhang, Q.H., Li, C.C., Shu, H.L., Ying, Y., Dai, Z.P., Wang, X., Liu, X.Y., Liang, A.M., Shen, H.X., Yi, B.Q., 2012. The impact of circulation patterns on regional transport pathways and air quality over Beijing and its surroundings. Atmos. Chem. Phys. 12, 5031–5053. https://doi.org/10.5194/acp-12-5031-2012.

Zhang, Q., Yuan, B., Shao, M., Wang, X., Lu, S., Lu, K., Wang, M., Chen, L., Chang, C.C., Liu, S.C., 2014. Variations of ground-level O_3 and its precursors in Beijing in summertime between 2005 and 2011. Atmos. Chem. Phys. 14, 6089–6101. https://doi.org/10.5194/acp-14-6089-2014.

Zhang, Y., Mao, H., Ding, A., Zhou, D., Fu, C., 2013. Impact of synoptic weather patterns on spatio-temporal variation in surface O_3 levels in Hong Kong during 1999–2011. Atmos. Environ. 73, 41–50. https://doi.org/10.1016/j.atmosenv.2013.02.047.

Zhang, Y., Ding, A., Mao, H., Nie, W., Zhou, D., Liu, L., Huang, X., Fu, C., 2016. Impact of synoptic weather patterns and interdecadal climate variability on air quality in the North China plain during 1980–2013. Atmos. Environ. 124, 119–128.

Zhao, Z., Wang, Y., 2017. Influence of the West Pacific subtropical high on surface ozone daily variability in summertime over eastern China. Atmos. Environ. 170, 197–204. https://doi.org/10.1016/j.atmosenv.2017.09.024.

Zhu, J., Xia, X., Che, H., Wang, J., Cong, Z., Zhao, T., Kang, S., Zhang, X., Yu, X., Zhang, Y., 2019. Spatiotemporal variation of aerosol and potential long-range transport impact over the Tibetan Plateau, China. Atmos. Chem. Phys. 19, 14637–14656. https://doi.org/10.5194/acp-19-14637-2019.